

SIMULATION OF THE 2001 PLANET-ENCIRCLING DUST STORM WITH THE NASA/NOAA MARS GENERAL CIRCULATION MODEL. R. J. Wilson¹, R.M. Haberle², J. Noble², A.F.C. Bridger², J. Schaeffer², J.R. Barnes³, and B.A. Cantor⁴. ¹NOAA/Geophysical Fluid Dynamics Laboratory, Princeton, NJ 08542 (John.Wilson@noaa.gov), ²Space Science Division, NASA/Ames Research Center, Moffett Field CA, 94035, ³College of Oceanic and Atmospheric Sciences, Oregon State University, Corvallis, OR. 97331, ⁴Malin Space Science Systems, San Diego, CA, 92191-0148.

Introduction: An outstanding problem for simulating the present Mars climate is representing the spatial and temporal variability of aerosols and the feedbacks that connect dust raising and transport with the evolving atmospheric circulation. The detailed MGS observations of the 2001 Martian global dust storm has provided the first opportunity to study the initiation and growth of a major planet-encircling dust storm with multiple sets of high spatial and temporal resolution data [1,2,3]. This paper describes a synthesis of MOC imagery and TES opacity and temperature retrievals to provide a description of the initiation and evolution of the 2001 planet encircling dust storm. We additionally make use of Mars general circulation model (MGCM) simulations to obtain insight into the atmospheric circulation at the time of storm initiation and its subsequent evolution in response to greatly increased solar heating. This study includes an investigation of mechanisms involving radiative-dynamical feedbacks associated with lofted dust. The MGCM provides a means of relating the observed dust opacity and temperature fields, while additionally providing a self-consistent atmospheric circulation. The circulation is critical for testing hypotheses for storm initiation and growth.

The TES opacity and temperature observations have recently been assimilated into the UK-MGCM [4,5]. TES dust opacity and atmospheric temperature sounding provide constraints on the simulated temperature fields, which control the atmospheric circulation. Our approach is complementary to that effort. We supplement the TES opacity observations with MOC imagery and allow the simulated dust distribution to evolve, while the column opacity is constrained by the observations. The UK model assimilation assumes a specified vertical structure for the aerosol field while we allow this to freely evolve. In this manner we attempt to assimilate the observed opacities. Note however that our simulation is unconstrained by the observed temperatures. Both efforts seek to investigate the radiative feedback between the evolving circulation and dust-driven radiation.

Storm Summary: Figure 1 summarizes the development of equatorial temperature structure during the period of the dust storm. The TES observations have been zonally averaged. The storm began with small dust storms local to the Hellas region similar to those that

occur during the recession of the south polar ice cap every spring. Expansion began in earnest at $L_s = 184.7^\circ$ when lifting spread northward across the equator into Syrtis Major, and eastward into the Hesperia and Promethei. Dust lifted east of Hellas also spread southward over the seasonal polar cap, and eastward toward the southern reaches of the Tharsis bulge. Meanwhile, separate lifting centers became active in Syria and Solis Planum. MOC images and TES opacity data demonstrate this progression. New lifting centers then developed in the Elysium region of the northern hemisphere, and in the Claritas region of southern Tharsis. By the end of the expansion phase ($L_s = 192.7$), the lifting region in Claritas/Thaumasia expanded southward toward the polar cap, westward into Daedalia, and eastward into Solis, with a combined lifting area roughly equivalent to that of the Hellas region, which by now appeared diffuse and no longer a source region.

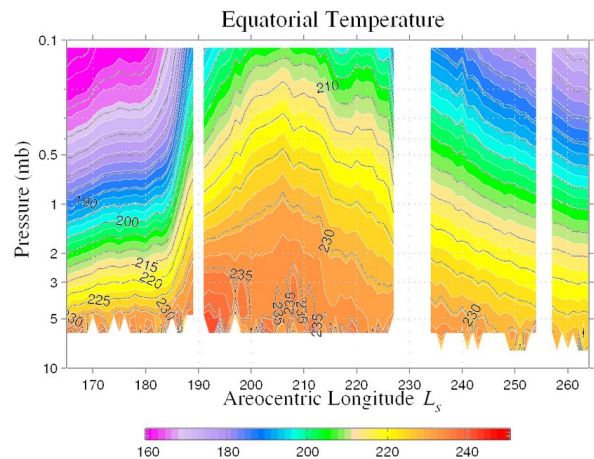


Figure 1. Evolution of zonally-averaged equatorial (5°S-5°N) daytime (1400 LT) temperature derived from TES temperature retrievals.

Although dust was being transported across Hesperia towards the east and had reached the western edge of the Tharsis plateau by $L_s = 188^\circ$, the imaging and the TES optical depth data suggest that the activation of a secondary dust lifting center in Syria Planum

immediately preceded the rapid storm growth to global encircling scale by $L_s \sim 190^\circ$.

The bulk of the dust added to the atmosphere during the mature phase came from the south Tharsis region where lifting is believed to have continued until $L_s = 242^\circ$, a span of 84 sols from the time lifting first began in Claritas [1]. By the time global opacities peaked at $L_s = 212^\circ$, a diffuse and now global dust haze obscured much of the planet's surface. Clearing to conditions more typical of years without such a storm took another 80 sols.

Mars general circulation model: The NASA/NOAA Mars GCM is based on the atmospheric dynamical cores and associated code infrastructure that is part of the GFDL Flexible Modeling System. The new MGCM is being adapted to work with physics parameterizations developed at both GFDL and NASA/Ames. The dynamical core employs finite volume (FV) numerics featuring conservative flux-form semi-Lagrangian horizontal discretization with monotonic constraints, and a terrain-following Lagrangian control-volume vertical coordinate that simplifies vertical advection calculations while maintaining high order numerical accuracy. The FV dynamical core has been implemented with two grid geometries; a latitude-longitude grid typical of most climate models and a cubed-sphere grid, which provides for relatively uniform spatial coverage and avoids the computational issues associated with the convergence of meridians of longitude. The modeling described here uses the cubed-sphere grid with a resolution of $2^\circ \times 2^\circ$. The current model uses the suite of physical parameterizations employed by the predecessor GFDL Skyhi-based MGCM [6] and the NASA/Ames radiation code (see other presentations). The advection scheme can transport an arbitrary number of tracer constituents that are used to represent the particle size distributions of dust aerosol, water vapor, and cloud ice. The model includes parameterizations for dust lifting, but these are not employed in the current simulations.

Our simulations are based on our best estimates of the evolving column dust opacity. These are primarily based on the TES optical depth retrievals, but are supplemented by consideration of MOC imagery and surface temperature data. The model carries a radiatively active dust tracer that is constrained by the specified evolving, spatially-variable column opacity. This constraint is applied only when and where valid observations are available. Differences between predicted and observed dust column opacity are reconciled by adding or removing dust from the model boundary layer.

Observations and Simulations: The precursor phase is characterized by a series of seven quasi-periodic dust "pulses" seen in the MOC imagery that developed along the edge of the retreating south polar cap mostly in and around the southwestern portion of

the Hellas basin. These pulses contributed to a gradual increase in the overall dustiness of the Hellas region and are probably the main contributor to the slight rise in global opacities at the end of this phase. The persistent action of local dust lifting within Hellas following the "seeding" event just after $L_s = 177^\circ$ appears critical to the initiation of the 2001 global dust storm.

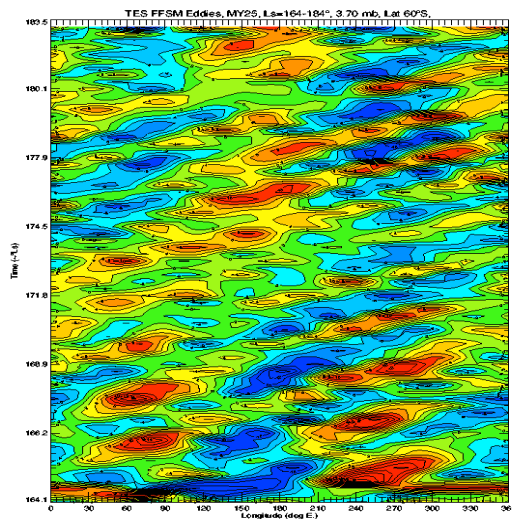


Figure 2. Hovmoller diagram showing the propagation of eddies at 60° S. TES temperatures observations at 3.7 hPa have been processed with the Fast Fourier Spectral Mapping method [7]. The time axis runs from $L_s = 164^\circ$ to $L_s = 184^\circ$.

An analysis of TES temperature data (Figure 2) indicates the presence of eastward propagating waves. We hypothesize that this triggering is related to the constructive interference of eastward propagating traveling waves with the diurnally varying tidal/slope wind system within and around the Hellas basin. These waves have a period of ~ 2 sols which suggests a possible synchronization with the diurnal tide. This interpretation is consistent with the UK-MGCM TES assimilation results [5]. Our simulations indicate that traveling waves can strongly modulate the diurnally-varying stress in the SW corner of the Hellas basin. We do find that simulated traveling waves are sensitive to the structure of the SH polar vortex. Inclusion of radiatively active water ice clouds over the south polar hood appears to yield more realistic polar temperature structure.

After $L_s = 185^\circ$, dust moved out of the Hellas region and global temperatures began to rapidly increase, as seen in Figure 1. This certainly would require significant vertical transport. The result was an amplified

zonal wave 1 pattern in midlevel (~ 0.5 hPa) temperature.

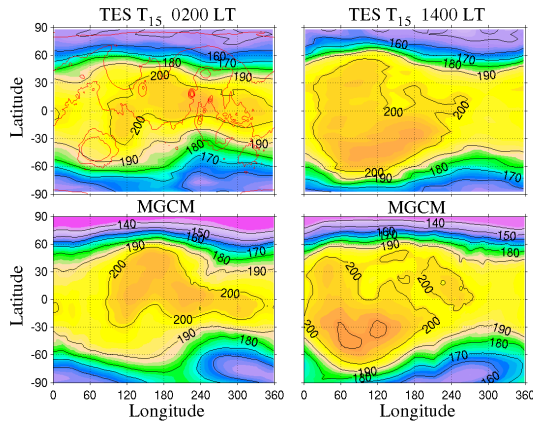


Figure 3. Latitude-longitude variation of midlevel (~ 0.5 hPa) temperature at $L_s = 187.5^\circ$ derived from TES retrievals (top) and a MGCM simulation (bottom). Morning temperatures (0200 LT) are shown in the left column and afternoon (1400 LT) temperatures are shown in the right column.

Figure 3 shows the observed and simulated and 0.5 hPa temperature response to the dust outbreak from Hellas that was well developed by $L_s = 187^\circ$. The close agreement suggests the dust heating has been well-approximated in the simulation. A latitude-height cross section of the simulated temperature and dust fields is shown in Figure 4. The diurnal mean circulation is one with two latitudinally extended Hadley cells of comparable intensity characterize the eastern hemisphere with rising motion close to the equator and poleward motion aloft. The aerosol field serves as a tracer for the circulation, which is found to have a significant diurnal variation. The simulated circulation indicates that strong daytime winds on the northern rim of Hellas and in Hesperia are responsible for dust transport into the core of the Hadley circulation updraft at the equator.

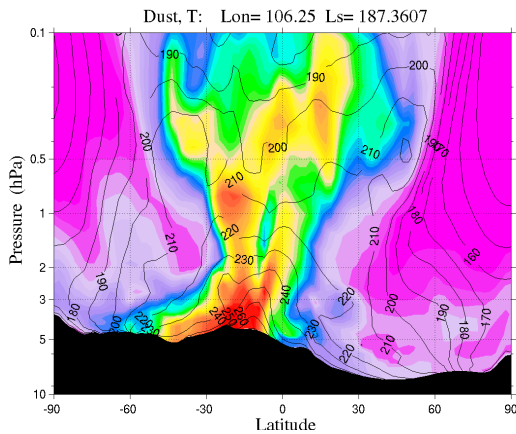


Figure 4. Latitude-height cross section of simulated afternoon (1400 LT) aerosol and temperature at 106° E longitude for $L_s = 187.5^\circ$, the same period illustrated in Figure 3. Temperature is contoured at intervals of 10 K and dust mixing ratio is shaded.

Of course the circulation is three-dimensional and the rising dust plume in the tropics rapidly extends downstream to the east as a consequence of the development of a tropical westerly flow.

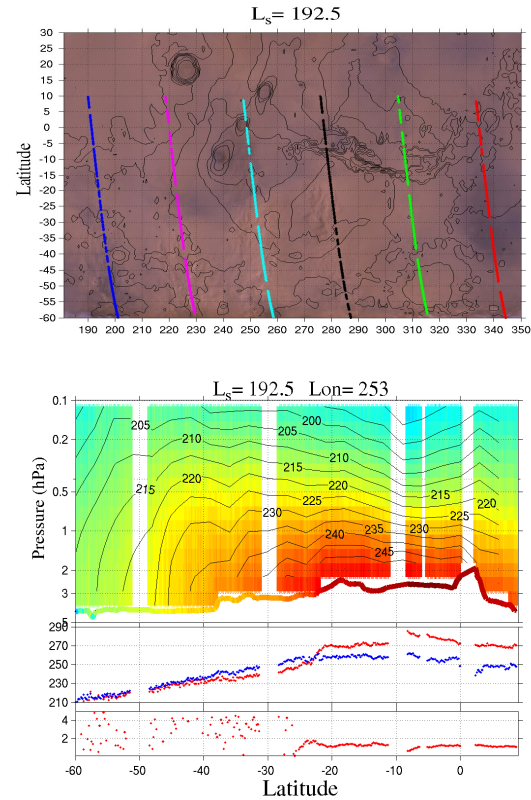


Figure 5. (a) MOC image of the dust cloud in Solis Pluum and Thaumasia. Individual spacecraft orbits are also shown. (b) Temperature cross-section derived from TES retrievals from the cyan orbit. (c) The corresponding surface (red) and near-surface air temperature (blue). (d) The derived TES dust opacity. Reliable opacity retrieval is dependent on a temperature contrast between the atmosphere and the surface. MOC image courtesy of H. Wang.

Figure 5 shows a MOC image of the dust storm well into the expansion stage. There is an extensive region of structured dust cloud in the Claritas/Thaumasia region with a prominent frontal feature oriented SW-NE. This feature is not so evident in the TES air temperatures but is revealed as a jump in the surface/air temperature contrast. Figure 6 shows simulated cross-sections of temperature, dust and meridional wind that correspond to the cross-section shown in Figure 5b. There is a shallow, intense equatorward flow that appears to be consistent with the imagery in Figure 5a. This flow is dominated by the thermal tide and results in strong daytime equatorial convergence and upward motion in the tropics. The strong vertical

shear in the wind field may partially account for the fine “billowy” cloud top structure in Figure 5b. Interestingly, some of the strongest wind stresses in the simulation are associated with intense nighttime downslope winds. The initiation of the 1977a dust storm monitored by Viking was likely associated with a very extensive morning dust cloud that was observed in Thaumasia ($\sim 40^\circ$ S) [8].

Together with Figure 4, it is clear that there are likely significant variations in the vertical structure of the aerosol field, thus illustrating the utility of allowing the structure of the aerosol field to evolve with the model circulation. Figure 7 shows the low-level tide wind amplitude at four times during the storm expansion. There is a strong amplification of the tide winds as the dust loading increases.

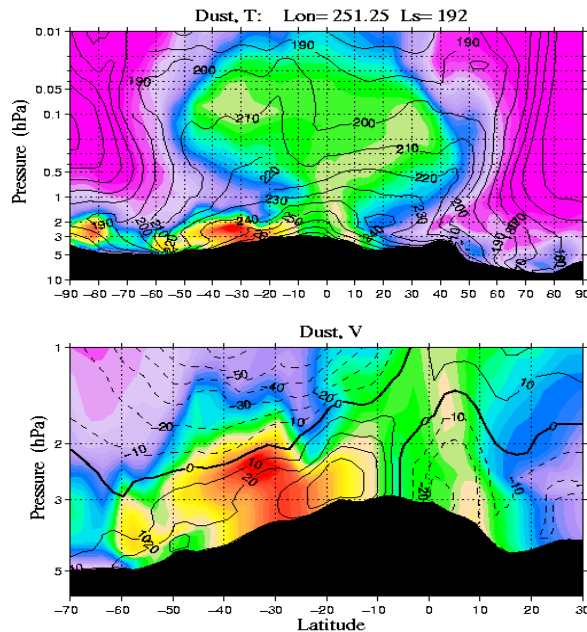


Figure 6. (a) Same as Figure 4 but for 252° E longitude at $L_s = 192.5^\circ$. Note the deeper domain. This section corresponds to that illustrated in Figure 5. Note the differences in latitude and height extent. (b) Zoom view of dust mixing ratio (shaded) and meridional wind velocity, contoured at intervals of 10 ms^{-1} .

Conclusions and Future Work: We have found that allowing the MGCM to self-consistently advect a radiatively active dust distribution, suitably constrained by the observed column opacity, allows a realistic simulation of atmospheric temperature evolution. The Hadley circulations and the thermal tides play a prominent role in structuring the aerosol field. An unusual aspect of this storm is its very early occurrence in the Mars year. Numerical simulations of dust storm conditions [9] have typically emphasized solstice con-

ditions, when the Hadley circulation and the associated subtropical SH westerly jet are predicted to be most intense and can most efficiently transport dust raised throughout the SH. The coupling of the low-level thermal tide (Fig. 7a) with the lower branch of the Hadley circulation evidently plays a critical role in moving dust raised in Hellas to the tropics where it can be globally distributed by the rising branch of the Hadley circulation. The eastward expansion of the storm and initiation of new lifting sites the Tharsis region appears to be consistent with the amplification of the thermal tide.

We find that the simulation of traveling waves during the initiation state of the storm simulations is sensitive to the structure of the SH polar vortex. A similar sensitivity is evident in an assessment of the UK-MGCM assimilation results.

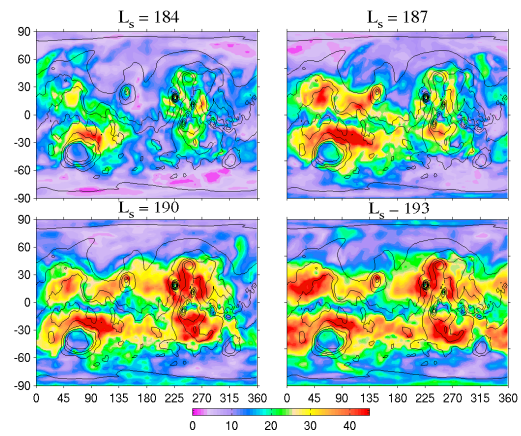


Figure 7. The evolution of the spatially varying pattern of tide wind amplitude at ~ 300 m above ground.

We are continuing to refine our estimates of the evolving column opacity distribution with which to force new simulations. We plan to introduce a distribution of dust particle sizes to obtain a more realistic representation of the aerosol field. We intend to make comparisons with simulations employing dust lifting parameterizations based on surface stress.

References: [1] Cantor B. A. (2007) *Icarus*, 186, 60–96. [2] Smith M. D. (2004) *Icarus*, 167, 148–165. [3] Straussberg et al. (2005) *JGR*, 110, E02006, 10.1029/2004JE002361. [4] Montabone, L. et al. (2006) *Icarus*, 185, 113–132 [5] Montabone, L. et al. (2008) Abstract in this issue. [6] Hinson, D., and R.J. Wilson (2004) *JGR* 109, E01002. [7] Barnes, J.R. (2006) Proceedings Second International workshop on Mars atmosphere modeling and observations, Granada, Spain, 2006. [8] Briggs et al. (1979) *JGR* 84, 2795–2820. [9] Basu, S. et al. (2006), *JGR.*, 111, E09004, doi:10.1029/2005JE002660.